Anisotropy and Coarsening in the Instability of Solid Dewetting Fronts

M. Dufay and O. Pierre-Louis

LPMCN, Université Lyon 1, 43 boulevard du 11 novembre 1918, 69622 Villeurbanne, France

(Received 22 October 2010; published 11 March 2011)

We report on the destabilization of the film edge during the dewetting of ultrathin solid films. An unusual coarsening behavior is found within the linear instability regime. In addition, we find that the instability is suppressed along faceted orientations. Our results are obtained via kinetic Monte Carlo simulations. An analytical model based on diffusion-limited mass transport on the rim and nucleation-limited increase of the rim height provides a good description of kinetic Monte Carlo simulations. Our results are consistent with recent experimental observations.

DOI: 10.1103/PhysRevLett.106.105506 PACS numbers: 81.10.Aj, 68.55.−a

Dewetting, the process by which a continuous film breaks up into droplets or islands, has been studied in many systems, including liquids, polymers, and solids. Dewetting is known to produce a complex dynamical behavior, with a wide variety of regimes and instabilities [1,2]. Since thin solid films play a major role in nanotechnologies, much effort has been devoted to the understanding of their stability. Solid films with various materials exhibit specific dewetting dynamics, where mass transport is limited by surface diffusion [3–7]. In recent experiments with nanometrically thin SOI films (Si/SiO_2), large scale ordered arrays of islands emerging from the dewetting process were observed [4,8–10]. In these experimental studies, dewetting is usually initiated at the film edge, or at point defects. A rim forms in the initial stages [11]. Then, the rim destabilizes, leading to an array of fingers which finally breakup into islands. Anisotropy plays a crucial role in this scenario, since it controls the birth [4,12] and the final orientation [4,10] of the fingers.

In this Letter, we discuss the early stages of the dewetting process and analyze the stability of the rim. Our study is based on a kinetic Monte Carlo (KMC) model which has been recently shown to be in good agreement with experiments in SOI systems [10]. We also present an analytical model which accounts for the main features of KMC simulations. We show that an instability emerges for rough front orientations, while fronts along faceted orientations remain stable. In addition, unstable fronts exhibit an unusual coarsening behavior within the linear regime. This instability ultimately leads to the breakup of the rim, and suggests a size selection mechanism for fingers and islands.

We first present the solid-on-solid KMC model [13,14]. Adsorbate atoms are placed on a square lattice, with lattice parameter a, and periodic boundary conditions. The local height is $z = 0, 1, 2, \ldots$ ($z = 0$ for the bare substrate, which is perfectly flat and frozen). Atoms hop to nearest neighbors, with the frequency $\nu = \nu_0 e^{-(nJ-\delta_z E_S)/T}$, where ν_0 is an attempt frequency, n is the number of in-plane nearest neighbors, J is the bond energy, T is the temperature normalized with the Boltzmann constant, and $\delta_z = 1$ for atoms in contact with the substrate, $\delta_z = 0$ otherwise. The dimensionless parameter E_S/J is related to the energy cost for covering the substrate with the adsorbate [15]: $E_S/J = (E_{AV} + E_{AS} - E_{SV})/(2E_{AV})$, where E_{AV}, E_{AS}, and E_{SV} are the adsorbate-vacuum, adsorbate-substrate, and substrate-vacuum energies, respectively. Assuming that energies are not very different from free energies, we find $E_S/J \approx 0.35$ for SOI systems using experimental [12] and tight-binding model results [16]. In addition, for an accurate description of the step stiffness, J can be related to the kink energy ϵ via the relation $J = 2\epsilon$. Averaging over A and B step orientations on Si(100) [17], we find $T/J \approx 0.33$ for SOI systems. Recently, dewetting experiments have also been performed for Pt(111) films on Yttria-stabilized ZrO_2, and on Si_3N_4 [18]. Combining experimental measurements [18] and *ab initio* calculations [19], one finds $E_S/J \approx 0.7$ for both substrates, and $T/J \approx 0.2$.

In the following, we rescale energies with J, time with ν_0^{-1}, and space with a. Our KMC simulations are performed at $T = 0.4$ [20], and start with a straight trench in a continuous film of thickness $h = 3$. The trench widens, giving rise to two dewetting fronts moving in opposite directions. Snapshots of the simulations are shown on Fig. 1. A rim with a faceted top always forms in the early stages of the dynamics. The sides of the rim top facet define two lines, which will be denoted as $x_1(y, t)$ on the substrate side, and $x_2(y, t)$ on the film side, as shown on Fig. 2(a). When the initial trench is in the (100) direction, as in Fig. 1(a), we observe no instability, even at very long times $t > 10^9$ in large systems (with lateral size $L = 1200$). However, fronts along the (110) direction exhibit an instability of x_1, while x_2 remains straight, as shown in Fig. 1(b). The wavelength of the instability—measured with the number of extrema of the front, is reported on Fig. 2(c), and increases with time. The amplitude of the instability also grows, ultimately leading to the breakup of the rim. Finally, fingers emerge and invade the film, as shown in Fig. 1(c).

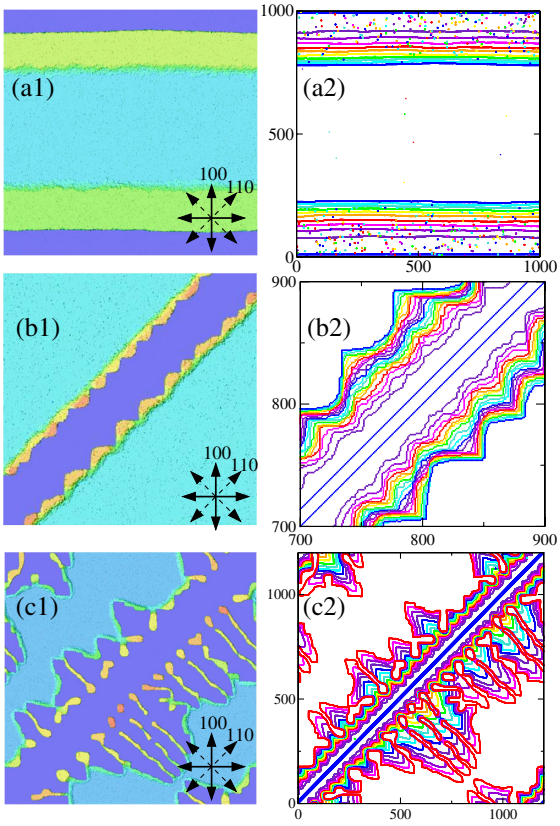

FIG. 1 (color online). KMC simulations. Snapshots are presented in the left panels, here the Gray-scale (blue-yellow-red color scale online) indicates the local height z. Right panels show the evolution of the film edge position x_1 as a function of time. Dewetting fronts are initiated by trenches along (100) in (a), along (110) in (b),(c). In all cases $T = 0.4$, and the initial height is $h = 3$. (a) A straight faceted rim forms, and no instability is observed for the (100) front, in a 1000×1000 system, with $E_S = 0.5$. (b) Zoom (200×200) at the early stages along (110). The typical wavelength of the instability increases with time: one observes coarsening. (c) Late time dynamics of (110) fronts. Fingers emerge from the rim instability. Parameters for (b),(c) 1200×1200 system, with $E_S = 1.5$.

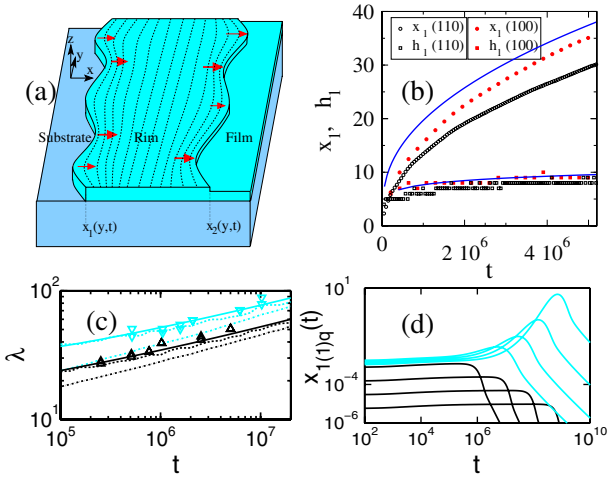

FIG. 2 (color online). Model results (except for E_S, the parameters are the same as in Fig. 1). (a) Mechanism of the instability. Dashed lines are isoconcentration lines, and arrows indicate diffusion mass fluxes. (b) Straight front solution (solid blue line) compared to the average motion of (100) and (110) fronts from KMC simulations (symbols) for $E_S = 1$. (c) Typical wavelength of the instability for $E_S = 1$ (gray or blue online) and $E_S = 2$ (black). The symbols are the instability wavelength from KMC simulations calculated from the number of maxima of the front. The solid line corresponds to Eq. (11), the dashed line and the dash-dotted lines account for the wavelength of the instability calculated from the solution of Eq. (9), with the number of maxima or the wavelength of maximum amplitude, respectively. (d) Evolution of the amplitude of different modes. One observes instability for (110) fronts (gray or blue online, $q = 0.25, 0.16, 0.1, 0.06$). Modes with smaller qs exhibit a larger peak at later times, leading to coarsening. In contrast, (100) fronts (black $q = 0.05$, 6×10^{-4}, 8×10^{-6}, 10^{-7}) are stable: the amplitude saturates for some time, and then decreases.

Two remarks are in order. First, we found no qualitative change in the parameter range $0.5 < E_S < 2$ and $0.3 < T < 0.6$ (simulations with $E_S < 0.5$, or $T < 0.3$ were too slow to be performed systematically). Second, experiments in SOI systems [12] exhibit an anisotropy similar to that observed in KMC simulations, where the instability is suppressed when the front is rotated by 45°. In the following, we analyze the stability in the two directions, and show that the stability of the (100) front results from the presence of a (100) vertical facet at the rim edge on the substrate side (x_1).

So far, most theoretical investigations of the dewetting process in the literature have been based on the isotropic continuum surface-diffusion model of Mullins [21]. Such an approach has allowed one to study the opening of holes in the film [22], and the motion and stability of films and straight dewetting fronts [23,24]. However, there is not only experimental evidence of strongly anisotropic behaviors [4,12], but also evidence of the presence of facets on the dewetting rim [10,25]. The dynamics on these facets, which is related to 2D nucleation, cannot be described within the Mullins model. Thus, another model [14], including diffusion-limited mass transport on the rim facet and nucleation-limited increase of the rim facet height, was proposed recently. In Ref. [14], the global motion of the straight faceted (100) front in KMC simulations was shown to be well described by this model. We here extend this model to describe the full 2D dynamics of the dewetting rim, including the possible instabilities. Mass conservation on the rim facet now reads

$$h_1 v_{n1} = -\mathbf{n}_1 \cdot D\nabla c_1 + \ell \partial_t h_1, \tag{1}$$

$$h_2 v_{n2} = -\mathbf{n}_2 \cdot D\nabla c_2, \tag{2}$$

where h_1 is the rim facet height, $h_2 = h - h_1$, the indices $i = 1, 2$ refers to the fronts x_1, x_2, and $\ell = x_2 - x_1$. In addition, v_{ni} are normal velocities along the normal vector $\mathbf{n}_i$ (towards the film). The adatom concentration c of the top facet obeys a quasistatic diffusion equation $D\Delta c = 0$.

At the fronts $i = 1, 2$, the concentration c is fixed to its equilibrium value $c_i = c_{\rm eq} e^{\mu_i/T}$, where μ_i are the local chemical potentials [15]:

$$\mu_1 = -\tilde{\gamma}_1 \kappa_1 + E_S/h_1, \tag{3}$$

$$\mu_2 = \tilde{\gamma}_2 \kappa_2. \tag{4}$$

Here κ_i is the front curvature, and $\tilde{\gamma}_i = \tilde{\gamma}_{fi}/h_i$, where $\tilde{\gamma}_{fi}$ is the total stiffness of the front i.

In addition, the rim height increases via 2D nucleation on the rim facet. Using nucleation theory, and diffusion-limited step dynamics, one finds [14]:

$$\partial_t h_1 = \frac{\ell^{1/2}}{h_1^{7/4}} \frac{D c_{\rm eq} C_{\rm zip}^{1/2} E_S^{7/4}}{\pi^{1/2} \gamma^{3/2} T^{1/4}} e^{-\pi \gamma^2 h_1/(2TE_S)}, \tag{5}$$

where $C_{\rm zip} \approx 0.25$, and γ is the step free energy on the rim facet.

Solving this model for a straight rim, one finds $x_1, x_2 \sim t^{1/2}$, with small corrections related to the slow dynamics of h_1 [14]. The solution is in good agreement with the global motion of the stable (100) front, but also with that of the (110) front (before the rim breakup) in KMC simulations with no fitting parameter, as shown on Fig. 2(a).

In order to discuss the morphological stability of the dewetting front, the model equations are linearized as

$$c(x, y, t) = c_{(0)}(x, t) + c_{(1)}(x, y, t), \tag{6}$$

$$x_i(y, t) = x_{i(0)}(t) + x_{i(1)}(y, t), \tag{7}$$

$$h_1(y, t) = h_{1(0)}(t) + h_{1(1)}(y, t), \tag{8}$$

where $i = 1, 2$. The quantities with the index (0) are the straight front solution, and (1) indicates a small perturbation. Upon the substitution of Eqs. (6)–(8) into the model Eqs. (1)–(5), we obtain a linear system of equations to leading order in the perturbation. We define q as the Fourier wave vector along y. The Fourier components obey the following dynamical equation

$$\partial_t \xi_q(t) = \mathbf{M}_q(t) \xi_q(t), \tag{9}$$

where $\xi_q(t) = (x_{1(1)q}(t), x_{2(1)q}(t), h_{1(1)q}(t))$, and $\mathbf{M}_q(t)$ is a time-dependent 3×3 matrix which depends on the 0th order straight front solution. The lengthy expression of the coefficients of $\mathbf{M}_q(t)$ will be reported in a forthcoming publication.

We choose the initial rim width ℓ_{2*} to be the width at the time t_{2*} of completion of the second rim layer, assuming that the first rim layer was formed with a width $\ll \ell_{2*}$, where t_{2*} and ℓ_{2*} are calculated from the model of Ref. [14]. We also assume that the fronts 1 and 2 roughen as if they were in equilibrium during t_{2*}. Assuming diffusion-limited dynamics, the initial Fourier amplitudes then obey [26]: $|x_{i(1)q}(0)|^2 = (1 - e^{-t_{2*}/\tau_i})(T/\gamma q^2 L h_{i*})$, with $\tau_i = T h_{i*}/(4 D c_{\rm eq} \tilde{\gamma}_i q^3)$, where $h_{1*} = h + 2$, and $h_{2*} = 2$, while the phases are randomly chosen. In addition, since the rim facet is atomically flat in the straight unperturbed front [14], we choose $h_{1(1)}(x, 0) = 0$.

Let us first focus on the case of the unstable (110) orientation. Since the (110) orientation is rough, we assume that $\tilde{\gamma}_1 = \tilde{\gamma}_2 = \gamma$. This assumption amounts to considering (110) fronts as bunches of isotropic steps, neglecting entropic interactions. The full numerical solution of the linearized model (9) is performed using 5000 Fourier modes. An instability of $x_{1(1)}$ appears, while the amplitude of $x_{2(1)}$ remains small, in agreement with KMC simulations. The mechanism of the instability is depicted in Fig. 2(a), and can be interpreted as a diffusion-limited destabilization similar to the Bales and Zangwill [26], or Mullins and Sekerka [26] instabilities. In order to compare the full numerical solution of Eq. (9) with KMC simulations, we use [13,14]: $\gamma = 0.42$ J, and $D c_{\rm eq} = e^{-2J/T}/4$. The typical wavelength of the instability in the full numerical solution, shown in Fig. 2(c), is in agreement with KMC simulations. Changing the details of the initial conditions only have small consequences on the result.

We now proceed with a more detailed analysis of Eq. (9). From the mechanism depicted in Fig. 1, the instability is expected to occur at $q\ell \gg 1$, and the term $\partial_t h_{1(1)}$ in Eq. (1) is expected to be irrelevant. Within this limit $h_{1(1)q}(t) = 0$, and $\mathbf{M}$ is diagonal. The resulting dynamics can be solved as

$$x_{i(1)q}(t) = x_{i(1)q}(0) e^{q(\sigma_i a_i(t) - b_i(t) q^2)}, \tag{10}$$

where $a_i(t) = \int_0^t dt' (D c_{\rm eq} E_S/T) h_{1(0)}^{-1}(t') h_{i(0)}^{-1}(t') \ell_{(0)}^{-1}(t')$, $b_i(t) = \int_0^t dt' (D c_{\rm eq} \tilde{\gamma}_i/T) h_{i(0)}^{-1}(t')$, $\sigma_1 = +1$, and $\sigma_2 = -1$.

The contribution proportional to $b_i(t)$ related to the front stiffness is always stabilizing, while the contribution proportional to $\sigma_i a_i(t)$ is destabilizing for x_1 and stabilizing x_2, as expected from Figs. 1(a) and 2(b). Since the increase of h_1 is exponentially attenuated from Eq. (5), we may obtain a simple qualitative picture by assuming that $h_{1(0)}(t)$ is constant. Such an assumption leads to $b_i(t) \sim t$, and $a_i(t) \sim \int dt \ell^{-1} \sim t^{1/2}$. As a consequence, the destabilizing term is always dominant at short times, and the stabilizing term is always dominant at large times. Hence, $x_{1(1)q}$ exhibits a maximum in time, shown in Fig. 2(d). This maximum depends on q. As a consequence, the wavelength of the mode of largest amplitude $\lambda_{\rm max}$ increases with time, leading to coarsening. At long times, the consequences of initial conditions are negligible and

$$\lambda_{\rm max} \approx 2\pi \left(\frac{3 \int_0^t dt' \tilde{\gamma}_1 h_{1(0)}^{-1}(t')}{\int_0^t dt' E_S h_{1(0)}^{-2}(t') \ell_{(0)}^{-1}(t')} \right)^{1/2}. \tag{11}$$

If $h_{1(0)}(t)$ were constant, one would have $\ell \sim t^{1/2}$, and $\lambda_{\rm max} \sim t^{1/4}$. However, due to the slow increase of h_1, one obtains an effective power law $\lambda \sim t^{0.2}$ from Eq. (11), in agreement with the full numerical solution of the model, and with KMC simulations, as shown in Fig. 2(c).

We now introduce the consequences of the term $\partial_t h_{1(1)}$ of Eq. (1) in perturbation. The resulting expressions are lengthy, and will be reported elsewhere. They indicate that $x_{2(1)}$ is in phase with $x_{1(1)}$, while $h_{1(1)}$ is out of phase with it, in qualitative agreement with KMC simulations. Indeed, the wider parts of the rim are higher than the pinched parts, and x_2 exhibits a small waviness in phase with x_1 in Fig. 1(b).

From the full numerical solution of Eq. (9), we have observed the breakup of the rim when the typical perturbation amplitude becomes equal to ℓ. Breakup occurs with a typical wavelength λ_B, after a time t_B, with

$$t_B \sim E_S^{-2.8} h^{4.2}, \qquad \lambda_B \sim E_S^{-1.0} h^{1.2}. \tag{12}$$

However, we could not confirm these scalings with KMC simulations due to the high computational cost of the simulations. Once again these results can be understood if we assume that $q\ell \gg 1$, and h_1 is constant, leading to

$$t_B \approx \frac{3^6 T \tilde{\gamma}_1^2 h_1^4 h^3}{2^7 D c_{\mathrm{eq}} E_S^3 (h_1 - h)^3}, \qquad \lambda_B \approx \frac{3^2 \pi \gamma h_1 h}{2 E_S (h_1 - h)}. \tag{13}$$

Using the additional assumption that $h_1 \sim h$, we obtain $t_B \sim E_S^{-3} h^4$ and $\lambda_B \sim E_S^{-1} h$. These results are in reasonable agreement with the full numerical solution Eqs. (12). At this point, it is tempting to speculate that the rim breakup at the wavelength λ_B selects the width of the fingers which evolve in the fully nonlinear regime.

We now turn to the case of (100) fronts. Here, we do not claim quantitative accuracy, and we rather focus on a qualitative discussion of the stability. Our starting point is the observation of the presence of a vertical (100) facet at x_1 in (100) fronts. As an approximation, vertical steps running on the vertical (100) facet may then play the same role as kinks in atomic steps. The energy of such steps is of the order of γh_1, where γ is the step free energy, so that the step density per unit (100) front length reads $n_s \approx 2e^{-\gamma h_1/T}$. Since n_s is low, the front diffusivity can be calculated as $\beta^2 \approx n_s$ [27]. The diffusivity can in turn be related to an effective stiffness [27] $\tilde{\gamma}_{100} = T/\beta^2 \approx (T/2)e^{\gamma h_1/T}$. The exponential increase of $\tilde{\gamma}_{100}$ with h_1 is expected, because a true facet without steps running on it should emerge when h_1 becomes large. Hence, $\tilde{\gamma}_1 = \tilde{\gamma}_{100}/h_1$ increases drastically during the dewetting process where h_1 increases. The full solution of Eq. (9) then indicates that the front should be stable, as shown in Fig. 2(d), and in agreement with KMC simulations of Fig. 1(c). This can be understood from the simplified expression of Eq. (10), where the stabilizing term $b_i(t)$ increases exponentially with h_1.

Finally, we would like to make some link with previous work on rim stability, discussed within the frame of the isotropic continuum surface-diffusion model of Mullins. In Ref. [24], the instability was considered as emerging from a frozen rim, and this strong assumption forbade the appearance of coarsening. It is therefore tempting to speculate that a full stability analysis of the dewetting rim within the Mullins model should also lead to coarsening, although the coarsening exponent could be different. In addition, the instability was interpreted as the consequence of the energy-minimizing Rayleigh-Plateau instability of the rim in Ref. [24]. In contrast, our interpretation summarized on Fig. 2(a) classifies the rim instability as a diffusive kinetic instability similar to the Mullins and Sekerka, or Bales and Zangwill instabilities [26].

In conclusion, dewetting fronts exhibit an instability where coarsening can be observed within the linear regime. We also find a strong anisotropy of the instability, which is consistent with experiments in SOI systems [12].

We acknowledge support from ''Nanomorphogénèse'' and ''DéFiS'' ANR-PNANO grants.

[1] P. G. de Gennes, Rev. Mod. Phys. **57**, 827 (1985).
[2] R. V. Craster and O. K. Matar, Rev. Mod. Phys. **81**, 1131 (2009).
[3] E. Jiran and C. Thompson, Thin Solid Films **208**, 23 (1992).
[4] B. Yang *et al.*, Phys. Rev. B **72**, 235413 (2005).
[5] B. Krause *et al.*, J. Chem. Phys. **119**, 3429 (2003).
[6] R. Saxena *et al.*, Phys. Rev. B **72**, 115425 (2005).
[7] M. Coll *et al.*, Phys. Rev. B **73**, 075420 (2006).
[8] Danielson *et al.*, J. Appl. Phys. **100**, 083507 (2006).
[9] Z. Burhanudin *et al.*, Thin Solid Films **508**, 235 (2006).
[10] E. Bussman *et al.*, report, 2010 (to be published).
[11] R. Nuryadi, Y. Ishikawa, Y. Ono, and M. Tabe, J. Vac. Sci. Technol. B **20**, 167 (2002).
[12] D. Danielson, Ph.D. thesis, University of California, Berkeley, 2001.
[13] O. Pierre-Louis, A. Chame, and Y. Saito, Phys. Rev. Lett. **99**, 136101 (2007).
[14] O. Pierre-Louis, A. Chame, and Y. Saito, Phys. Rev. Lett. **103**, 195501 (2009).
[15] O. Pierre-Louis, A. Chame, and M. Dufay, Eur. Phys. J. B **77**, 57 (2010).
[16] J. H. Wilson, J. D. Todd, and A. P. Sutton, J. Phys. Condens. Matter **2**, 10 259 (1990).
[17] N. C. Bartelt, R. M. Tromp, and E. D. Williams, Phys. Rev. Lett. **73**, 1656 (1994).
[18] H. Galinski *et al.*, Phys. Rev. B **82**, 235415 (2010).
[19] P. Feibelman, Surf. Sci. **463**, L661 (2000).
[20] This precise choice is motivated by our quantitative knowledge of the step free energy at $T = 0.4$ [13,14].
[21] W. Mullins, J. Appl. Phys. **28**, 333 (1957).
[22] D. Srolovitz and S. Safran, J. Appl. Phys. **60**, 255 (1986).
[23] H. Wong *et al.*, Acta Mater. **48**, 1719 (2000).
[24] W. Kan and H. Wong, J. Appl. Phys. **97**, 043515 (2005).
[25] E. Dornel *et al.*, Phys. Rev. B **73**, 115427 (2006).
[26] C. Misbah, O. Pierre-Louis, and Y. Saito, Rev. Mod. Phys. **82**, 981 (2010).
[27] See, e.g., Y. Saito, *Statistical Physics of Crystal Growth* (World Scientific, Singapore, 1996).